# TE-TM mode coupling in two-dimensional photonic crystals composed of liquid-crystal rods

Hiroyuki Takeda and Katsumi Yoshino
*Department of Electronic Engineering, Graduate School of Engineering, Osaka University, 2-1 Yamada-oka, Suita, Osaka 565-0871, Japan*
(Received 23 February 2004; published 13 August 2004)

We theoretically demonstrate the TE-TM mode coupling in two-dimensional photonic crystals composed of liquid-crystal rods due to anisotropies of liquid crystals. In such structures, the classification of the TE and TM modes is generally impossible, that is, the TE-TM mode coupling occurs. Frequencies of the mode coupling are investigated by the plane-wave expansion method, and the mode coupling is discussed by transmittance calculated by the finite-difference time-domain method. Changes of transmittance by rotating directors of liquid crystals are also discussed.

DOI: 10.1103/PhysRevE.70.026601 PACS number(s): 42.70.Qs

## I. INTRODUCTION

Recently, photonic crystals with dielectric periodic structures have attracted much attention from theoretical and experimental viewpoints [1,2]. The photonic crystals have photonic band gaps in which light in a certain frequency range cannot propagate, and group velocities of light become zero at photonic band edges because of high dispersion relations between frequencies and wave vectors. Moreover, point and linear defects in photonic crystals with photonic band gaps cause light localization and guiding, respectively. That is, the point and linear defects can be viewed as cavities and waveguides, respectively [3,4]. Therefore, many researchers have devoted much effort to the development of photonic crystals.

On the other hand, it is important to obtain the tuning of optical properties in photonic crystals. Therefore, we have proposed various tunable photonic crystals composed of functional materials, such as conducting polymers whose optical properties can be controlled by temperature and electric fields [5,6]. In particular, dielectric indices of liquid crystals are changeable under the influence of electric fields. We experimentally proposed to use liquid crystals to photonic crystals and demonstrated tunable photonic crystals with synthetic opals and their replicas infiltrated with liquid crystals [6]. Theoretically, Busch and John supported the tunability of photonic crystals infiltrated with liquid crystals [7], and we have also proposed various unique tunable photonic crystals incorporated with liquid crystals [8,9].

In our previous paper, we discussed the TE-TM mode coupling in two-dimensional square-lattice photonic crystals composed of Si rods with surface defects of liquid crystals [9]. In this case, wide photonic band gaps and surface defect modes exist in the TM mode, while no clear photonic band gaps exist in the TE mode. We found that in the mode coupling, transmittance decreases sharply and mode conversion occurs at the photonic band edges and the surface defect modes in the TM mode, regardless of the input TE and TM waves. That is, the strong mode coupling occurs at frequencies of zero group velocities in the TM mode. In this model, the mode coupling occurs only at the surface defects of liquid crystals in two-dimensional photonic crystals. Thus far, however, the mode coupling throughout two-dimensional photonic crystals due to anisotropies of liquid crystals has not been studied.

In this paper, therefore, we discuss the TE-TM mode coupling in two-dimensional square-lattice photonic crystals composed of liquid-crystal rods. The TE and TM modes can be classified in the case of directors of liquid crystals parallel and perpendicular to two-dimensional planes. In the case of other directors, however, the TE and TM modes cannot be classified, that is, the mode coupling occurs. We investigate frequencies of the mode coupling by the plane-wave expansion (PWE) method [10], and discuss the mode coupling by transmittance in the $\Gamma$-$X$ and $\Gamma$-$M$ directions. The transmittance is calculated by the finite-difference time-domain (FDTD) method [11]. Changes of the transmittance by rotating directors of liquid crystals are also discussed.

## II. THEORY

Following Busch and John's discussion, we calculate two-dimensional photonic band structures composed of liquid-crystal rods by the PWE method [7,10]. The magnetic field $\mathbf{H}(\mathbf{r})$ satisfies the following equation from the Maxwell equations:

$$\nabla \times [\epsilon^{-1}(\mathbf{r}) \nabla \times \mathbf{H}(\mathbf{r})] = \frac{\omega^2}{c^2}\mathbf{H}(\mathbf{r}), \tag{1}$$

where $\omega$ and $c$ are the frequency and the speed of light in vacuum, respectively. The dielectric tensor $\epsilon_{i,j}(\mathbf{r})$ $(i,j=x,y,z)$ is two-dimensionally periodic with respect to lattice vectors, and therefore, $\epsilon_{i,j}(\mathbf{r})$ can be expanded by the Fourier series, as follows:

$$\epsilon_{i,j}(\mathbf{r}) = \sum_{\mathbf{G}} \epsilon_{i,j}(\mathbf{G}) \exp(i\mathbf{G}\cdot\mathbf{r}), \tag{2}$$

where $\mathbf{G}$ and $\epsilon_{i,j}(\mathbf{G})$ are the reciprocal lattice vector and the coefficient of the Fourier series, respectively. By Bloch's theorem, moreover, the magnetic field is

 

$$\mathbf{H}(\mathbf{r}) = \sum_{\mathbf{G}} \mathbf{h}(\mathbf{G})\exp\{i(\mathbf{k}+\mathbf{G})\cdot\mathbf{r}\}$$

$$= \sum_{\mathbf{G}} \sum_{\lambda=1}^{2} h^{\lambda}(\mathbf{G})\mathbf{e}_{\mathbf{G}}^{\lambda}\exp\{i(\mathbf{k}+\mathbf{G})\cdot\mathbf{r}\}, \tag{3}$$

where $\mathbf{k}$ is the wave vector, and $h^{\lambda}(\mathbf{G})$ and $\mathbf{e}^{\lambda}(\mathbf{G})$ are the amplitudes and the polarized vectors perpendicular to $\mathbf{k}+\mathbf{G}$, respectively. In the case of liquid-crystal rods parallel to the $z$ direction, $\mathbf{e}_{\mathbf{G}}^{1}$ and $\mathbf{e}_{\mathbf{G}}^{2}$ are (0,0,1) and $(-(k_y+G_y),k_x+G_x,0)/|\mathbf{k}+\mathbf{G}|$, respectively. Substituting Eqs. (2) and (3) into Eq. (1) results in the following equation:

$$\sum_{\mathbf{G}'} |\mathbf{k}+\mathbf{G}||\mathbf{k}+\mathbf{G}'| \times \begin{bmatrix} \mathbf{e}_{\mathbf{G}}^{2}\cdot\epsilon^{-1}(\mathbf{G}-\mathbf{G}')\cdot\mathbf{e}_{\mathbf{G}}^{2}, & -\mathbf{e}_{\mathbf{G}}^{2}\cdot\epsilon^{-1}(\mathbf{G}-\mathbf{G}')\cdot\mathbf{e}_{\mathbf{G}}^{1}, \\ -\mathbf{e}_{\mathbf{G}}^{1}\cdot\epsilon^{-1}(\mathbf{G}-\mathbf{G}')\cdot\mathbf{e}_{\mathbf{G}}^{2}, & \mathbf{e}_{\mathbf{G}}^{1}\cdot\epsilon^{-1}(\mathbf{G}-\mathbf{G}')\cdot\mathbf{e}_{\mathbf{G}}^{1}, \end{bmatrix} \times \begin{bmatrix} h^{1}(\mathbf{G}') \\ h^{2}(\mathbf{G}') \end{bmatrix} = \frac{\omega^2}{c^2}\begin{bmatrix} h^{1}(\mathbf{G}) \\ h^{2}(\mathbf{G}) \end{bmatrix}. \tag{4}$$

By solving the eigenvalue equation in Eq. (4), frequencies for certain wave vectors are obtained. In the PWE method, errors of photonic band structures with 441 plane waves are within 1%. Details are discussed in Refs. [7,10].

We consider the two-dimensional photonic crystal in Fig. 1. Shaded circles indicate the liquid-crystal rods. A liquid crystal has two kinds of dielectric indices. Light that has electric field perpendicular and parallel to directors of liquid crystals has the ordinary dielectric index $\epsilon_o$ and the extraordinary dielectric index $\epsilon_e$, respectively. The directors of liquid crystals can be controlled by the applied electric field. The director of liquid crystals is assumed to exist in the $xz$ plane; that is, the director is $\mathbf{n}=(\sin\theta,0,\cos\theta)$. $\theta$ indicates the angle relative to the $z$ axis. Then, the dielectric tensor is represented as follows:

$$\epsilon_{xx}(\mathbf{r}) = \epsilon_o(\mathbf{r})\cos^2\theta + \epsilon_e(\mathbf{r})\sin^2\theta, \tag{5a}$$

$$\epsilon_{yy}(\mathbf{r}) = \epsilon_o(\mathbf{r}), \tag{5b}$$

$$\epsilon_{zz}(\mathbf{r}) = \epsilon_o(\mathbf{r})\sin^2\theta + \epsilon_e(\mathbf{r})\cos^2\theta, \tag{5c}$$

$$\epsilon_{xz}(\mathbf{r}) = \epsilon_{zx}(\mathbf{r}) = \{\epsilon_e(\mathbf{r}) - \epsilon_o(\mathbf{r})\}\sin\theta\cos\theta. \tag{5d}$$

Other components of the dielectric tensor are zero. We consider $\theta$ from 0° to 15°, since we investigate large changes of optical properties by changing small angles.

$\mathbf{e}_{\mathbf{G}}^{2}\cdot\epsilon^{-1}(\mathbf{G}-\mathbf{G}')\cdot\mathbf{e}_{\mathbf{G}}^{1}$ and $\mathbf{e}_{\mathbf{G}}^{1}\cdot\epsilon^{-1}(\mathbf{G}-\mathbf{G}')\cdot\mathbf{e}_{\mathbf{G}}^{2}$ in Eq. (4) are zero in the case of $\epsilon_{xz}(\mathbf{r})=\epsilon_{zx}(\mathbf{r})=0$ at $\theta=0°$ and 90°, and therefore, the classification of the TE and TM modes is possible. Then, $(\Sigma_{\mathbf{G}}|h^{1}(\mathbf{G})|^2,\Sigma_{\mathbf{G}}|h^{2}(\mathbf{G})|^2)$ are (1,0) and (0,1) in the TE and TM modes, respectively. At $\theta\neq 0°$ or 90°, however, the mode coupling occurs, and $(\Sigma_{\mathbf{G}}|h^{1}(\mathbf{G})|^2,\Sigma_{\mathbf{G}}|h^{2}(\mathbf{G})|^2)\neq(1,0)$ and (0,1). In particular, $(\Sigma_{\mathbf{G}}|h^{1}(\mathbf{G})|^2,\Sigma_{\mathbf{G}}|h^{2}(\mathbf{G})|^2)$ becomes (0.5,0.5) at frequencies of the strong mode coupling. We judge the mode coupling by $(\Sigma_{\mathbf{G}}|h^{1}(\mathbf{G})|^2,\Sigma_{\mathbf{G}}|h^{2}(\mathbf{G})|^2)$.

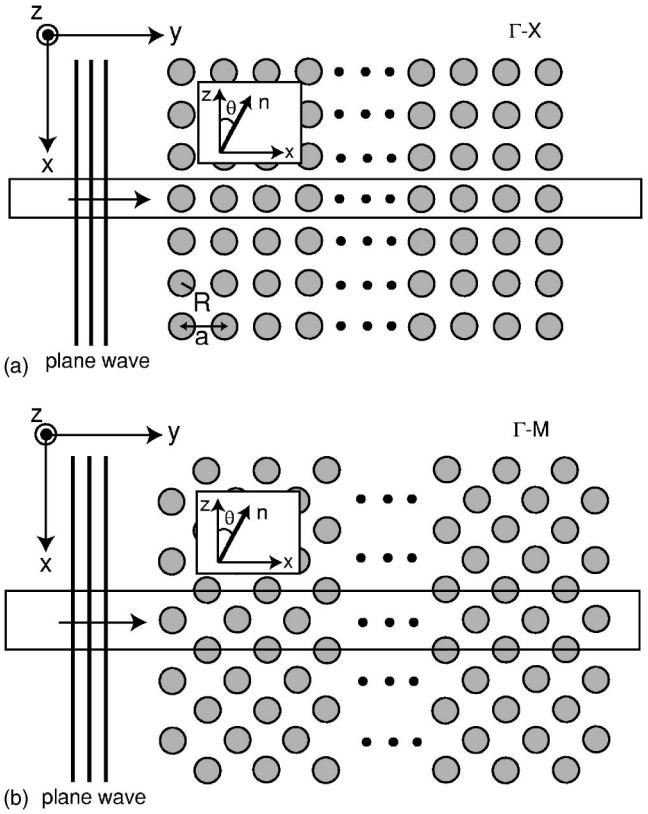


FIG. 1. Schematic diagram of two-dimensional square-lattice photonic crystals composed of liquid-crystal rods. Plane waves are assumed to be incident in the (a) Γ-$X$ and (b) Γ-$M$ directions. $R$ and $a$ indicate the radius of rods and the lattice constant, respectively. $\mathbf{n}$ and $\theta$ indicate the director of liquid crystals and the angle relative to the $z$ axis, respectively.

Moreover, we calculate transmittance in the Γ-X and Γ-M directions by the FDTD method [11]. In the FDTD method, higher accuracies and stabilities are obtained with increasing discrete time and lattices. The discrete time and lattices are $c\Delta t/a=0.0125$ and $\Delta x/a=\Delta y/a=0.025$, respectively. $a$ is the lattice constant of square lattices. These parameters satisfy $c\Delta t\leqslant\{(1/\Delta x)^2+(1/\Delta y)^2\}^{-1/2}$, which compensates the calculational stability. The number of time steps in this calculation is 50 000, and errors are within 1%. As shown in Figs. 1(a) and 1(b), input plane waves are assumed to be incident in the Γ-$X$ and Γ-$M$ directions, respectively, and we detect output electromagnetic waves on the right side of the photonic crystals in Fig. 1. Flows of the electromagnetic waves are defined by the Poynting vectors. In this paper, the only input TE wave is considered, and then, the output TE and TM waves are obtained. The output TM waves are obtained due to the mode coupling by anisotropies of liquid crystal. In the uniform media, the Poynting vectors of the input TE wave and the output TE and TM waves are as follows:

$$P_{TE}^{in} = \frac{1}{2}\eta|H_z^{in}(\omega)|^2, \tag{6a}$$

$$P_{TE}^{out} = \frac{1}{2}\eta|H_z^{out}(\omega)|^2, \tag{6b}$$

$$P_{TM}^{out} = \frac{1}{2\eta}|E_z^{out}(\omega)|^2; \tag{6c}$$

$\eta = \sqrt{\mu_0/(\epsilon_0\epsilon)}$ is the wave impedance, and $\epsilon_0$ and $\epsilon$ are the permittivity of free space and the dielectric constant of the uniform media, respectively. $H_z^{in}(\omega)$, $H_z^{out}(\omega)$, and $E_z^{out}(\omega)$ are the Fourier transform of electromagnetic waves. Transmittance of the output TE and TM waves for the input TE wave is

$$T_{TE-TE} = \frac{P_{TE}^{out}}{P_{TE}^{in}}, \tag{7a}$$

$$T_{TE-TM} = \frac{P_{TM}^{out}}{P_{TE}^{in}}, \tag{7b}$$

respectively.

In Figs. 1(a) and 1(b), the photonic crystals are assumed to have 15 and 21 layers, respectively. The regions embedded by solid lines indicate the calculational regions. The perfect matched layers are imposed as absorbing boundary conditions at the left and right sides of the calculational regions, and periodic boundary conditions are imposed at the top and the bottom of the calculational regions.

### III. NUMERICAL CALCULATION AND DISCUSSION

Let us consider the two-dimensional square-lattice photonic crystal composed of liquid-crystal rods, as shown in Fig. 1. The background is assumed to be air. Such a condition could be realized by silica aerogels. Silica aerogels are porous structures and diameters of pores are about 20 nm. Refractive indices of silica aerogels are about 1.03, that is, they are almost the same as that of the air. Optical absorption of hydrophobic silica aerogels occurs around the infrared region [12]. Therefore, the hydrophobic silica aerogels are useful in the visible range. Indeed, hydrophobic silica aerogels are used as very low refractive-index materials [13]. That is, the two-dimensional photonic crystals composed of liquid-crystal rods can be prepared by making a periodic array of holes in the silica aerogel plate and then infiltrating liquid crystals into holes.

When diameters of the holes are about 1 $\mu$m and are much larger than those of pores, liquid crystals could be trapped into the drilled holes. In making the holes in the silica aerogel plate by laser, moreover, pores around the holes may be broken by the heat of laser. Then, we do not have to consider the leak of liquid crystals into the pores around the holes. An experimental fabrication of tunable two-dimensional photonic crystals infiltrated with liquid crystals has already been reported [14].

Liquid crystals with large anisotropies are necessary so that photonic band structures show clear differences in the TE and TM modes. We assumed the liquid crystal with the ordinary index $n_o = 1.590$ and the extraordinary refractive index $n_e = 2.223$. This liquid crystal corresponds to the phenylacetylene type liquid crystal [15]. In Fig. 1, $R$ and $a$ indicate the radius of rods and the lattice constant, respectively, and we assume $R/a = 0.3$.

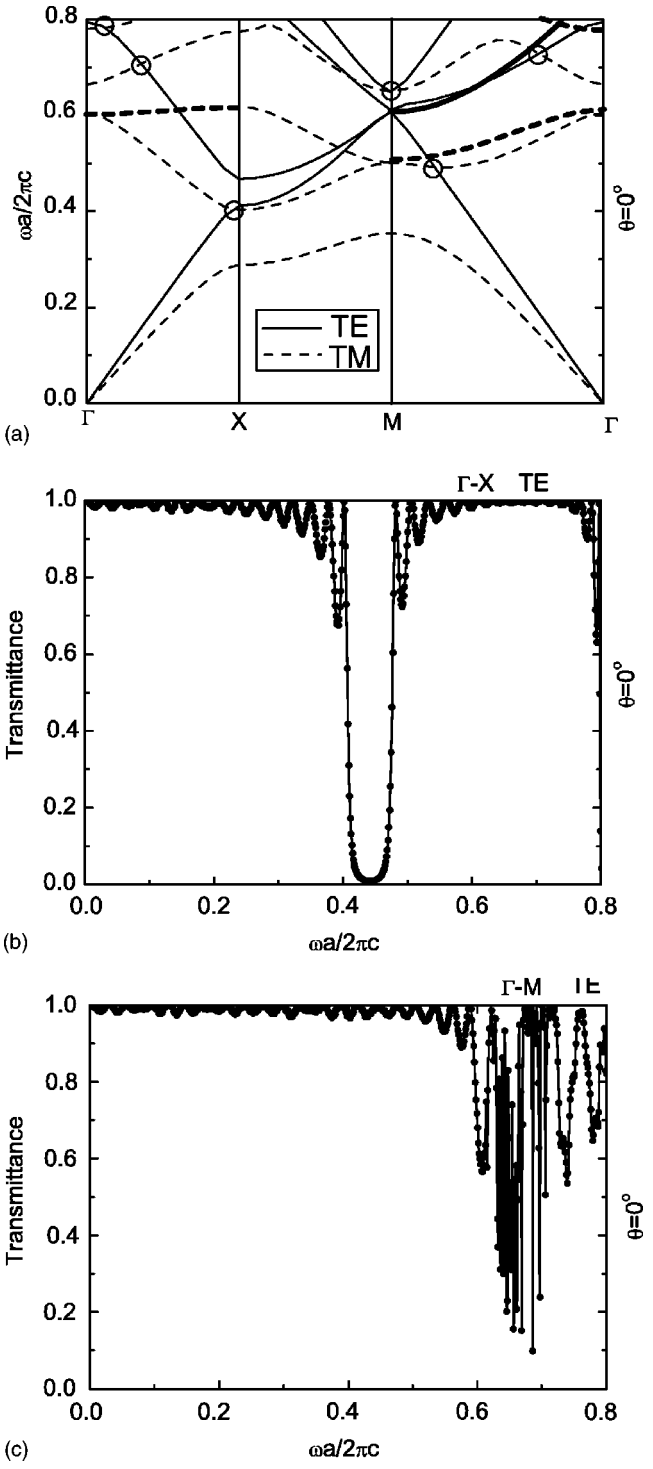


FIG. 2. (a) Photonic band structures in the TE and TM modes at $\theta = 0°$. Solid and dotted lines indicate the TE and TM modes, respectively. The photonic bands drawn by thick lines are uncoupled modes. Circles indicate the strong mode coupling. (b) and (c) Transmittance at $\theta = 0°$ in the $\Gamma$-$X$ and $\Gamma$-$M$ directions, respectively, in the TE mode.

In Fig. 2(a), we show the photonic band structure in the TE and TM modes at $\theta = 0°$. At $\theta = 0°$, the mode coupling does not occur. Solid and dotted lines indicate the TE and TM modes, respectively. The photonic bands drawn by thick

lines are uncoupled modes in which external plane waves cannot excite because of antisymmetric electromagnetic distribution [16]. As shown in this figure, the photonic band structure in the TM mode has higher dispersion relations between frequencies and wave vectors than that in the TE mode.

Although the TE and TM modes cannot be classified at $\theta \neq 0°$, the strong mode coupling is not obtained generally because of small angles, $0° \leqslant \theta \leqslant 15°$. However, we found that the strong mode coupling occurs at frequencies of intersection points of the TE and TM modes, that is, $(\Sigma_{\mathbf{G}}|h^1(\mathbf{G})|^2, \Sigma_{\mathbf{G}}|h^2(\mathbf{G})|^2)$ becomes (0.5, 0.5), as mentioned in Sec. II. We investigated the mode coupling in the $\Gamma$-$X$ and $\Gamma$-$M$ directions. In Fig. 2(a), circles indicate the strong mode coupling. In the $\Gamma$-$X$ direction, the circles exist around $\omega a/2\pi c = 0.40$, 0.71, and 0.78, while in the $\Gamma$-$M$ direction, the circles exist around $\omega a/2\pi c = 0.50$, 0.65, and 0.73. However, we note that the strong mode coupling does not occur at frequencies of intersection points of thick and thin lines due to differences of symmetry by uncoupled modes.

First, we discuss transmittance in the case of the mode noncoupling. As shown in Fig. 2(a), the photonic band structure in the TE mode has low dispersion relations in comparison with that in the TM mode, and changes of transmittance in the TE mode for frequencies are small. We focus our attention on changes of transmittance for the input TE wave by rotating $\theta$.

Figures 2(b) and 2(c) show transmittance at $\theta = 0°$ in the $\Gamma$-$X$ and $\Gamma$-$M$ directions, respectively, in the TE mode. In Fig. 2(b), the transmittance in the $\Gamma$-$X$ direction has a clear photonic band gap, while in Fig. 2(c), that in the $\Gamma$-$M$ direction has no clear photonic band gaps. In particular, the transmittance in Fig. 2(c) exhibits complex behaviors in the frequency range of $(0.6-0.8)2\pi c/a$, due to several dispersion relations. These results coincide with the photonic band structure in Fig. 2(a).

Next, we discuss transmittance in the case of the mode coupling. Figure 3(a) shows the photonic band structure at $\theta = 15°$ in the $\Gamma$-$X$ direction. Since we cannot classify the TE and TM modes, we draw all of photonic bands by solid lines. However, this photonic band structure is similar to that in Fig. 2(a), and circles in Fig. 3(a) correspond to those in Fig. 2(a). As shown in this figure, in particular, a clear small gap appears at the circle around $\omega a/2\pi c = 0.71$.

Figures 3(b) and 3(c) show the transmittance at $\theta = 15°$ of the output TE and TM waves for the input TE wave, respectively, in the $\Gamma$-$X$ direction. In Fig. 3(b), the transmittance changes significantly around $\omega a/2\pi c = 0.71$ in comparison with that in Fig. 2(b). This frequency corresponds to that of the circle in Figs. 2(a) and 3(a). That is, the transmittance decreases because of the clear small gap by the strong mode coupling. Around frequencies of other circles, however, clear changes cannot be viewed in the transmittance. This is because it is difficult to obtain the clear changes at photonic band edges where the transmittance changes abruptly for frequencies. In Fig. 3(c), on the other hand, the transmittance shows no characteristic changes even around $\omega a/2\pi c = 0.71$, although the transmittance of the output TM mode is obtained due to the mode coupling. That is, the clear small gap by the strong coupling does not cause effective mode conversion.

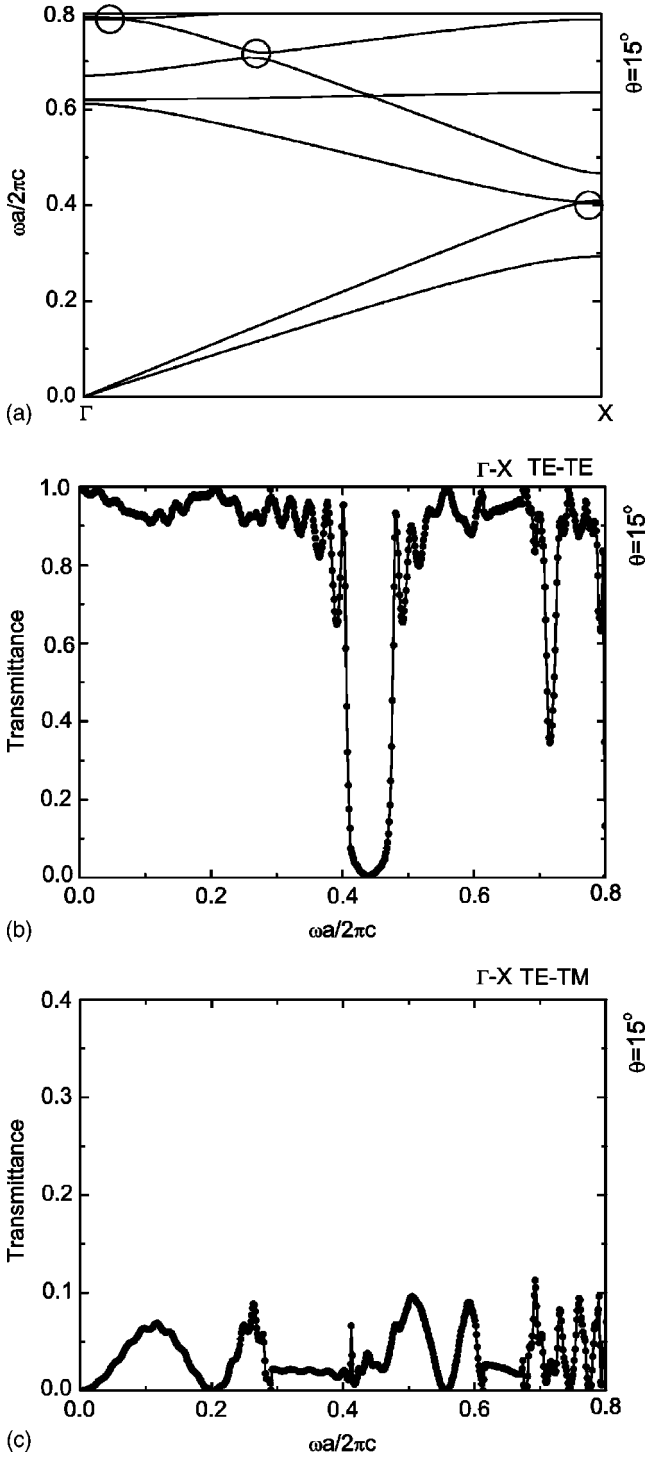


FIG. 3. (a) Photonic band structures at $\theta = 15°$ in the $\Gamma$-$X$ direction. Circles indicate the strong mode coupling. (b) and (c) Transmittance at $\theta = 15°$ of the output TE and TM waves for the input TE wave, respectively, in the $\Gamma$-$X$ direction.

Figure 4(a) shows the photonic band structure at $\theta = 8.5°$ in the $\Gamma$-$M$ direction. Since we cannot classify the TE and TM modes, as mentioned earlier, we draw all of photonic bands by solid lines. However, this photonic band structure is similar to that in Fig. 2(a), and circles in Fig. 4(a) correspond to those in Fig. 2(a). As shown in this figure, in particular, a

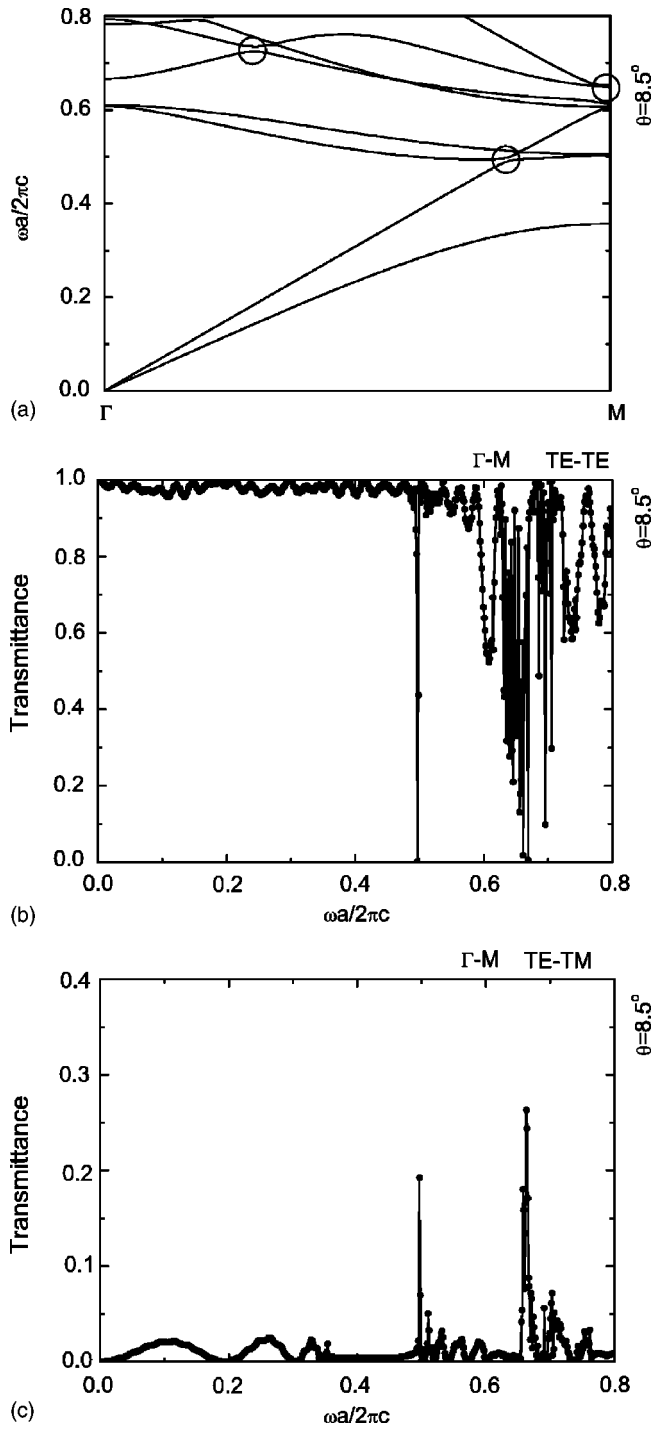


FIG. 4. (a) Photonic band structures at $\theta=8.5°$ in the $\Gamma$-$M$ direction. Circles indicate the strong mode coupling. (b) and (c) Transmittance at $\theta=8.5°$ of the output TE and TM waves for the input TE wave, respectively, in the $\Gamma$-$M$ direction.

clear small gap appears at the circle around $\omega a/2\pi c=0.73$.

Figures 4(b) and 4(c) show the transmittance at $\theta=8.5°$ of the output TE and TM waves for the input TE wave, respectively, in the $\Gamma$-$M$ direction. In Fig. 4(b), the transmittance changes sharply around $\omega a/2\pi c=0.5$ in comparison with that in Fig. 2(b). This frequency corresponds to that of the circle in Figs. 2(a) and 4(a). However, the transmittance shows no clear changes around frequencies of other circles because of several dispersion relations in the frequency of $(0.6-0.8)2\pi c/a$. In Fig. 4(c), on the other hand, the transmittance shows sharp peaks around $\omega a/2\pi c=0.5$ and 0.65. These frequencies correspond to those of the circles in Figs. 2(a) and 4(a). This is because in the photonic band structure in the TM mode, group velocities mostly become zero at these frequencies, as shown in Fig. 2. That is, significant changes occur because of the long mode coupling time. Around $\omega a/2\pi c=0.5$, in particular, the transmittance of the output TE wave becomes zero and that of the output TM wave shows the effective peak, which indicates mode conversion from the TE mode to the TM mode although transmission intensity decreases.

Figures 5(a)–5(c) show the photonic band structure at $\theta=15°$ and the transmittance at $\theta=15°$ of the output TE and TM waves for the input TE wave, respectively, in the $\Gamma$-$M$ direction. These figures correspond to Figs. 4(a)–4(c). As shown in Fig. 5(a), clear small gaps appear at the circles around $\omega a/2\pi c=0.5$ and 0.73.

In spite of the increasing of anisotropies of liquid crystals, the transmittance in Fig. 5(b) increases around $\omega a/2\pi c=0.5$ in comparison with that in Fig. 4(b), while the transmittance in Fig. 5(c) decreases around $\omega a/2\pi c=0.5$ in comparison with that in Fig. 4(c). This is because the clear small gap appears at the circle around $\omega a/2\pi c=0.5$, as shown in Fig. 5(a). As mentioned in Fig. 3(c), the mode conversion effect decreases by the clear small gap. Although there exists a frequency region without any photonic bands around $\omega a/2\pi c=0.71$ in Fig. 3(a), there exist no such frequency regions around $\omega a/2\pi c=0.5$ in Fig. 5(a). Unlike the transmittance around $\omega a/2\pi c=0.71$ in Fig. 3(b), therefore, that in Fig. 5(b) does not decrease around $\omega a/2\pi c=0.5$ in comparison with that in Fig. 4(b). On the other hand, the transmittance in Fig. 5(c) increases around $\omega a/2\pi c=0.65$ in comparison with that in Fig. 4(c) because of the increasing of anisotropies of liquid crystals. In this case, there are no clear small gaps around $\omega a/2\pi c=0.65$, as shown in Fig. 5(a).

In Figs. 6(a)–6(c), $\theta$ dependences of transmittance in the $\Gamma$-$X$ and $\Gamma$-$M$ directions are shown, respectively. Figure 6(a) shows the $\theta$ dependences of the transmittance of the output TE wave for the input TE wave around $\omega a/2\pi c=0.71$ in the $\Gamma$-$X$ direction. This frequency corresponds to that of the circle in Figs. 2(a) and 3(a). We do not consider the transmittance of the output TM wave because it shows no characteristic behaviors, as shown in Fig. 3(c). Black points indicate the transmittance of the output TE wave. The transmittance of the output TE wave decreases monotonically with increasing $\theta$. This is due to the increasing of the clear small gap by the strong coupling with increasing $\theta$, as shown in Fig. 3(a).

Figure 6(b) shows the $\theta$ dependences of the transmittance of the output TE and TM waves for the input TE wave around $\omega a/2\pi c=0.5$ in the $\Gamma$-$M$ direction. This frequency corresponds to that of the circle in Figs. 2(a), 4(a), and 5(a). Black and white points indicate the transmittance of the output TE and TM waves, respectively. With increasing $\theta$, the transmittance of the output TE wave decreases monotonically, and increases after becoming zero around $\theta=8.5°$. On the other hand, the transmittance of the output TM wave

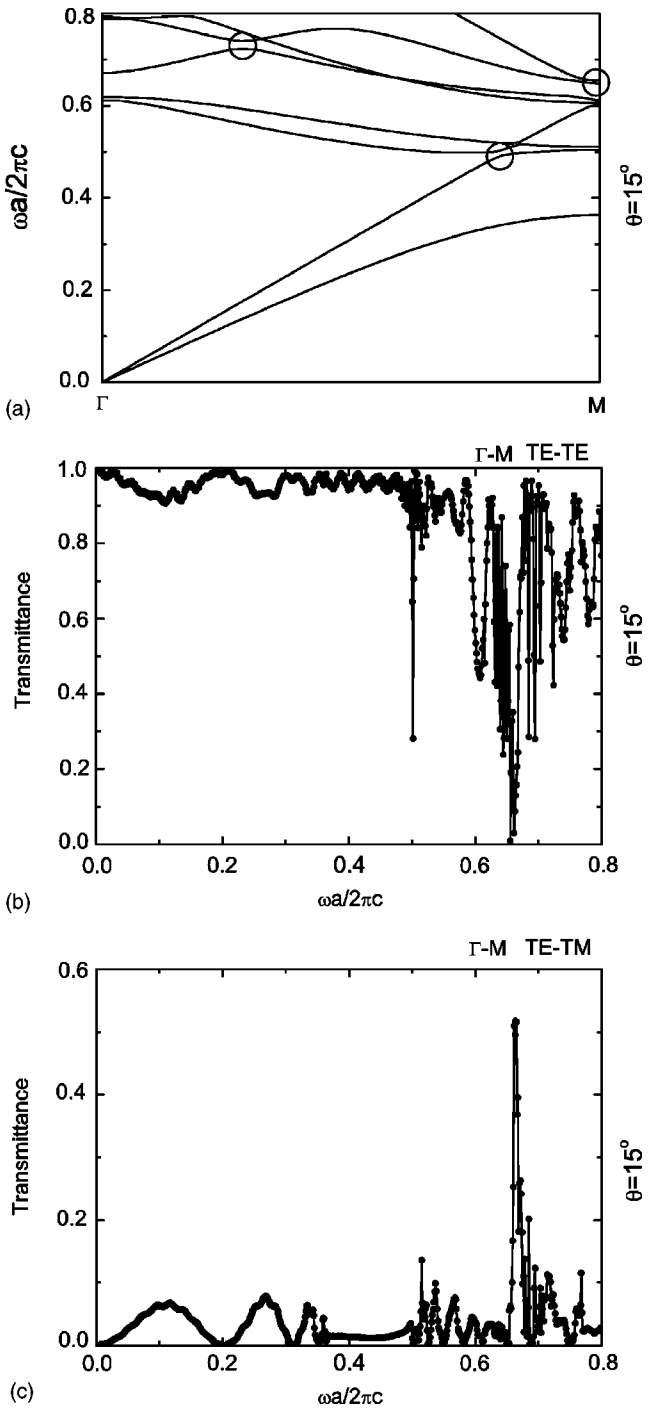


FIG. 5. (a) Photonic band structures at $\theta=15°$ in the $\Gamma$-$M$ direction. Circles indicate the strong mode coupling. (b) and (c) Transmittance at $\theta=15°$ of the output TE and TM waves for the input TE wave, respectively, in the $\Gamma$-$M$ direction.

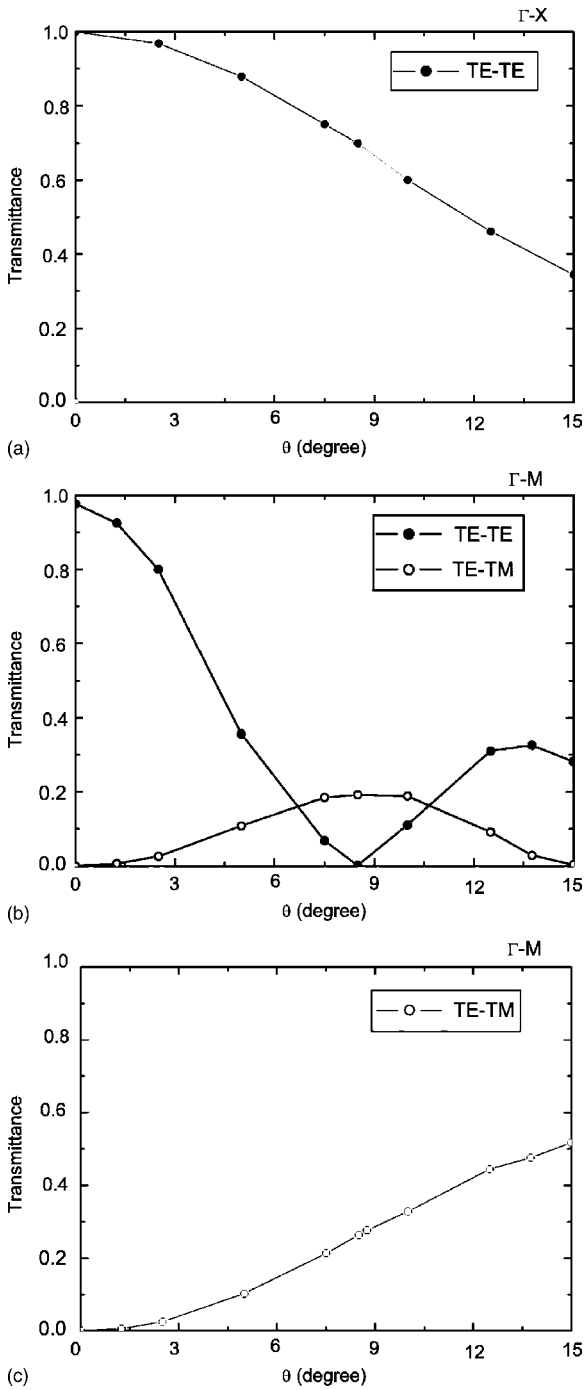


FIG. 6. $\theta$ dependences of transmittance in the (a) $\Gamma$-$X$ and (b), (c) $\Gamma$-$M$ directions. The considered frequencies are around $\omega a/2\pi c=$(a) 0.71, (b) 0.5, and (c) 0.65. Black and white points indicate the transmittance of the output TE and TM waves for the input TE wave, respectively.

becomes maximum around $\theta=8.5°$. With increasing $\theta$, both anisotropies of liquid crystals and the clear small gap around $\omega a/2\pi c=0.5$ increase. Although the former strengthens mode conversion effects, the latter weakens them. Therefore, the $\theta$ dependences of the transmittance show complex behaviors, as shown in Fig. 6(b).

Figure 6(c) shows the $\theta$ dependences of the transmittance of the output TM wave for the input TE wave around $\omega a/2\pi c=0.65$ in the $\Gamma$-$M$ direction. This frequency corresponds to that of the circle in Figs. 2(a), 4(a), and 5(a). We do not consider the transmittance of the output TE wave because it shows no clear changes, as shown in Figs. 4(b) and 5(b). White points indicate the transmittance of the output TM wave. The transmittance of the output TM wave increases monotonically with increasing $\theta$, that is, mode conversion effects increase. This is due to the increasing of

anisotropies of liquid crystals with increasing $\theta$. Because there are no clear small gaps in this case, the transmittance does not decrease.

From these results, the mode coupling occurs mainly at frequencies of intersection points of the TE and TM modes. In particular, the transmittance of the output TE wave changes sharply at frequencies of the intersection point of zero group velocities in the TM mode, while the transmittance of the output TM wave shows sharp peaks. However, clear small gaps by the strong mode coupling weaken mode conversion effects. This finding would provide applications to the sharp tuning at certain frequencies.

## IV. CONCLUSION

We theoretically demonstrated the TE-TM mode coupling in two-dimensional photonic crystals composed of liquid-crystal rods due to anisotropies of liquid crystals. The mode coupling mainly occurs at frequencies of intersection points of the TE and TM modes. By rotating $\theta$, the transmittance of the output TE wave changes greatly around $\omega a/2\pi c=0.71$ and 0.5 in the $\Gamma$-$X$ and $\Gamma$-$M$ directions, respectively. By rotating $\theta$, in particular, the effective mode conversion occurs at frequencies of the intersection points of zero group velocities in the TM mode. However, clear small gaps by the strong mode coupling weaken the mode conversion effects. This finding would provide applications to the sharp tuning at certain frequencies.

## ACKNOWLEDGMENTS

This work was partly supported by a Grant-in-Aid for Scientific Research from the Ministry of Education, Culture, Sports, Science and Technology and from the Japan Society for the Promotion of Science.

[1] E. Yablonovitch, Phys. Rev. Lett. **58**, 2059 (1987).
[2] S. John, Phys. Rev. Lett. **58**, 2486 (1987).
[3] R. D. Meade, A. Devenyi, J. D. Joannopoulos, O. L. Alerhand, D. A. Smith, and K. Kash, J. Appl. Phys. **75**, 4753 (1994).
[4] V. Kuzmiak and A. A. Maradudin, Phys. Rev. B **57**, 15242 (1998).
[5] K. Yoshino, S. B. Lee, S. Tatsuhara, Y. Kawagishi, M. Ozaki, and A. A. Zakhidov, Appl. Phys. Lett. **73**, 3506 (1998).
[6] Y. Shimoda, M. Ozaki, and K. Yoshino, Appl. Phys. Lett. **79**, 3627 (2001).
[7] K. Busch and S. John, Phys. Rev. Lett. **83**, 967 (1999).
[8] H. Takeda and K. Yoshino, Phys. Rev. B **67**, 073106 (2003).
[9] H. Takeda and K. Yoshino, Phys. Rev. E **68**, 046602 (2003).
[10] K. Busch and S. John, Phys. Rev. E **58**, 3896 (1998).
[11] A. Taflove and S. C. Hagness, *Computational Electrodynamics: The Finite-difference Time-domain Method* (Artech House, Boston, 1995).
[12] H. Yokogawa, J. Non-Cryst. Solids **186**, 23 (1995).
[13] T. Sumiyoshi, J. Non-Cryst. Solids **225**, 369 (1998).
[14] S. W. Leonard, J. P. Mondia, H. M. van Driel, O. Toader, S. John, K. Busch, A. Birner, U. Gosele, and V. Lehmann, Phys. Rev. B **61**, R2389 (2000).
[15] K. Fujisawa (private communication). (These liquid crystals with large anisotropies were developed by K. Fujisawa at Sumitomo Chemical with the support of the National Program of the Association of the Super Advanced Electronic Technology, supported by the Ministry of International Trade and Industry, Japan. We cannot show the evidence because of the patent procedure for a while.)
[16] K. Sakoda, Phys. Rev. B **52**, 7982 (1995).